Mode instability in one-dimensional anharmonic lattices: Variational equation approach

K. Yoshimura*
Department of Applied Mathematics and Physics, Kyoto University, Kyoto 606-8501, Japan
(Received 20 September 1996; revised manuscript received 1 September 1998)

The stability of normal mode oscillations has been studied in detail under the single-mode excitation condition for the Fermi-Pasta-Ulam-β lattice. Numerical experiments indicate that the mode stability depends strongly on k/N, where k is the wave number of the initially excited mode and N is the number of degrees of freedom in the system. It has been found that this feature does not change when N increases. We propose an average variational equation — approximate version of the variational equation — as a theoretical tool to facilitate a linear stability analysis. It is shown that this strong k/N dependence of the mode stability can be explained from the view point of the linear stability of the relevant orbits. We introduce a low-dimensional approximation of the average variational equation, which approximately describes the time evolution of variations in four normal mode amplitudes. The linear stability analysis based on this four-mode approximation demonstrates that the parametric instability mechanism plays a crucial role in the strong k/N dependence of the mode stability. [S1063-651X(99)03003-2]

PACS number(s): 45.05.+x, 05.45.−a, 05.20.−y

I. INTRODUCTION

The statistical mechanics is established on the assumption that every system will settle in an equilibrium state. One-dimensional anharmonic lattices form one of simple dynamical models to check this assumption. The study of the stability properties of nonequilibrium motion exhibited by one-dimensional anharmonic lattices was initiated by Fermi, Pasta, and Ulam [1] to numerically check whether the assumption is satisfied. They chose an initial condition far from equilibrium, giving all energy to the lowest frequency normal mode, and then numerically integrated the equations of motion, expecting that chaotic energy exchange among the normal modes was occurring because of anharmonicity of the lattice and the system was quickly relaxing to an equilibrium state characterized by energy equipartition. However, it is well known that evident relaxation to the equilibrium state did not occur within their observation time scale but quasi-periodic normal mode oscillation including only a few low frequency modes was observed. Their numerical experiments suggested that nonequilibrium motions can last for a reasonably long time in one-dimensional anharmonic lattices.

Since the appearance of their ground-breaking work, many studies have been carried out to understand the dynamics of such systems [2–14]. It is clarified that there is a certain energy threshold for a transition from weakly to strongly chaotic motion and the system relaxes to the equilibrium state in a small time scale when energy increases well above the threshold. Recently, a new interpretation of the energy threshold was proposed [11,12] and detailed study of the chaoticity transition at the threshold was done by using the Riemannian geometric description of Hamiltonian chaos [15–18]. However, it is not still clear how the time scale or the stability of nonequilibrium motions depends on initial conditions.

The simplest situation arising in the study of the stability properties of nonequilibrium motions in one-dimensional anharmonic lattices is that involving only a single-mode excitation or a narrow-packet excitation. In such a situation, only a single normal mode of some wave number k or a wave packet of small size δk with mean wave number k ($\delta k/k \ll 1$) is initially excited. For a system subjected to such initial conditions, the stability of this mode of wave number k is characterized by a time scale over which its energy is transferred to the other modes. It is important for the purpose of understanding the dynamics of one-dimensional anharmonic lattices to study how mode stability depends on the wave number k in a system with simple initial conditions of this form. However, even this simple stability problem is not yet fully understood and in fact the mechanism underlying the wave-number dependence of the mode stability has not yet been described nor even identified.

There are only a few works that study the above mentioned problems. Izrailev and Chirikov applied the resonance overlap criterion [3] (see also Ref. [19]) and determined the chaoticity limit, which is the energy density threshold distinguishing weakly and strongly chaotic motions, as a function of the wave number k for the Fermi-Pasta-Ulam (FPU) β lattice. They concluded that in the regime of small k (i.e., $k \ll N$, where N is the system size) normal modes become more unstable as k increases. Berman and Kolovskij approximated the FPU-β lattice using a nonlinear Schrödinger equation under the narrow packet condition $\delta k/k \ll 1$ and determined the chaoticity limit as a function of k [4]. They found that in the regime $N-k \ll N$, normal modes become more stable as k increases. These two works provide qualitative results on the wave-number dependence of the mode stability, and their theoretical analyses give an indication of the possible underlying mechanism.

In a previous paper, we obtained quite different results for the FPU-β lattice using both theoretical and numerical analysis [20]. This study, however, was restricted to the sys-

*Present address: NTT Communication Science Laboratories 2-4, Hikaridai, Seika-cho, Soraku-gun, Kyoto 619-0237, Japan. Electronic address: kazuyuki@cslab.kecl.ntt.co.jp

tem of size $N=128$. We found that mode stability intricately depends on the wave number k of the initially excited mode, contrary to the simple k dependence reported in the two above-mentioned works. Our results demonstrate that the instability of the normal mode is enhanced intermittently in some specific wave-number ranges. It is also demonstrated that normal modes possessing wave numbers within a certain range are extremely stable even at high energy density. The present paper reports further study on these phenomena, which is mainly addressed to two problems: (i) identifying the mechanism causing the strong wave-number dependence of the mode stability, and (ii) determining the effect on this strong wave-number dependence caused by an increase in the number N of degrees of freedom.

We carried out numerical experiments with N in the range 128–512 to investigate the effect caused by an increase in N. And, for the purpose of identifying the mechanism, we theoretically studied the mode stability using a linear stability analysis of the orbits that start from single-mode excitation initial conditions for various values of k. We approximate the relevant orbits with a Jacobi elliptic function and propose a variational equation valid along the approximate orbits as a theoretical tool to facilitate the linear stability analysis. It is shown that the linear stability of the approximate orbits is closely related to the mode stability and it explains the strong wave-number dependence of the mode stability quite well. Moreover, we carry out a detailed study on the mechanism responsible for the strong wave-number dependence. We rewrite the variational equation valid along the approximate orbits in the normal mode coordinates and introduce a four-mode approximation of it obtained by retaining only four mode components that are dominant in determining the linear stability. We show that a parametric instability mechanism of the four-mode variational equations is essentially responsible for the enhancement of instability and the existence of the highly stable modes.

The present paper is organized as follows. In Sec. II, we describe the FPU-β model and define the stability of the normal mode. The numerical method we employ to investigate the stability is also described. In Sec. III we report the results of numerical experiments showing the effects caused by increasing N on the mode stability. In Sec. IV we undertake a theoretical investigation of the mechanism responsible for the strong wave-number dependence of the mode stability through a linear stability analysis. Conclusions are offered in Sec. V.

II. DYNAMICAL MODEL AND STABILITY OF NORMAL MODE

In this section, we describe the FPU-β model, the normal modes, and we define the stability of normal mode oscillation. We also explain the manner in which this stability is numerically examined.

A. FPU-β model and normal mode

Our investigation is of the dynamical model described by the Hamiltonian

$$H=\frac{1}{2}\sum_{i=1}^{N-1} p_i^2+\sum_{i=1}^{N}\left[\frac{1}{2}(q_i-q_{i-1})^2+\frac{\beta}{4}(q_i-q_{i-1})^4\right]. \tag{1}$$

This is referred to as the FPU-β model. This Hamiltonian describes a one-dimensional anharmonic lattice with nearest neighbor interaction. The parameter β represents the nonlinear coupling strength. We will set $\beta=1$ in later discussion. We employ fixed-end boundary conditions, i.e., $q_0=q_N=0$. The equations of motion derived from the Hamiltonian (1) are

$$\frac{d^2q_i}{dt^2}=q_{i+1}+q_{i-1}-2q_i+\beta[(q_{i+1}-q_i)^3-(q_i-q_{i-1})^3]. \tag{2}$$

For convenience, we introduce normal mode coordinates. The transformation $\mathbf{q}\mapsto\mathbf{Q}$ defined by

$$q_i=\sqrt{\frac{2}{N}}\sum_{k=1}^{N-1} Q_k\sin\left(\frac{\pi k}{N}i\right)\quad (i=1,2,\ldots,N-1), \tag{3}$$

gives the normal modes of the corresponding harmonic system. Here, Q_k is the amplitude of the kth normal mode. The characteristic frequency of the kth normal mode is given as

$$\omega_k=2\sin\left(\frac{\pi k}{2N}\right). \tag{4}$$

In terms of the normal mode coordinates $\mathbf{Q}$ and their conjugate momenta $\mathbf{P}$, the Hamiltonian (1) is rewritten as

$$H=\sum_{k=1}^{N-1}\left(\tfrac{1}{2}P_k{}^2+\tfrac{1}{2}\omega_k{}^2Q_k{}^2\right)+\frac{\beta}{8N}\times\sum_{k_1,k_2,k_3,k_4=1}^{N-1}\omega_{k_1}\cdots\omega_{k_4}Q_{k_1}\cdots Q_{k_4}D(k_1,k_2,k_3,k_4), \tag{5}$$

where $D(k_1,k_2,k_3,k_4)$ represents the selection rule defining the interaction among the normal modes. It is explicitly written as

$$\begin{aligned}D(k_1,k_2,k_3,k_4)&=\delta(k_1+k_2,k_3+k_4)+\delta(k_1+k_3,k_2+k_4)\\&\quad+\delta(k_1+k_4,k_2+k_3)+\delta(k_1+k_2+k_3,k_4)\\&\quad+\delta(k_1+k_2+k_4,k_3)+\delta(k_1+k_3+k_4,k_2)\\&\quad+\delta(k_2+k_3+k_4,k_1)-\delta(k_1+k_2+k_3+k_4,2N)\\&\quad-\delta(k_1+k_2+k_3,2N+k_4)-\delta(k_1+k_2+k_4,2N+k_3)\\&\quad-\delta(k_1+k_3+k_4,2N+k_2)-\delta(k_2+k_3+k_4,2N+k_1),\end{aligned} \tag{6}$$

where δ is the Kronecker delta function. The equation of motion for the kth normal mode is

$$\frac{d^2}{dt^2}Q_k+\omega_k^2Q_k+\frac{\beta}{2N}\times\sum_{k_1,k_2,k_3=1}^{N-1}\omega_k\omega_{k_1}\omega_{k_2}\omega_{k_3}Q_{k_1}Q_{k_2}Q_{k_3}D(k,k_1,k_2,k_3)=0. \tag{7}$$

As the stability of the normal mode is the main subject of the present study, we must be clear about how we define the term ''stability.'' The initial conditions considered in the present study consist of a single-mode (or an almost single-mode) excitation: at the initial time, a single normal mode of wave number k is excited, and the amplitudes of the other modes are set to zero. Thus

$$Q_i(0)=\dot{Q}_i(0)=0 \quad (i\neq k). \tag{8}$$

The nature of these initial conditions implies that $Q_i(t)\simeq 0 (i\neq k)$ holds for a short period of time $t<\tau_s$, where τ_s is a time scale within which the single-mode oscillation of the kth mode lasts without significant energy being lost to the other modes. The time scale τ_s depends on the wave number k and the energy density ϵ, where ϵ is related to total energy E as $\epsilon=E/N$. We define the stability of the mode in terms of τ_s: an increase in τ_s corresponds to an increase in the normal mode stability. A method of estimating τ_s by numerical experiments will be described.

If the approximation $Q_i(t)=0 \ (i\neq k)$ is made in Eq. (7), the equation of motion for the kth normal mode (the mode excited initially) is approximated as

$$\frac{d^2}{dt^2}Q_k+\omega_k^2Q_k+\frac{3\beta}{2N}\omega_k^4{Q_k}^3=0. \tag{9}$$

It is well-known that the solution of Eq. (9) may be written, with the Jacobi elliptic function, in the form

$$\tilde{Q}_k(t)=a\sqrt{N}\,\mathrm{cn}(\sigma t,k_m), \tag{10}$$

where

$$a^2=\frac{4k_m^2}{3\beta{\omega_k}^2(1-2k_m^2)}, \quad \sigma^2=\frac{\omega_k^2}{1-2k_m^2}, \tag{11}$$

and k_m is the modulus of the Jacobi elliptic function. The modulus k_m is related to the energy density ϵ as

$$\epsilon=\frac{2k_m^2(1-k_m^2)}{3\beta(1-2k_m^2)^2}. \tag{12}$$

In phase space, the motion associated with $\tilde{Q}_k(t)$ defines the periodic orbit $\tilde{\mathbf{\Gamma}}(t)=[\tilde{\mathbf{q}}(t),\tilde{\mathbf{p}}(t)]$, where the components of $\tilde{\mathbf{q}}=(\tilde{q}_1,\ldots,\tilde{q}_{N-1})$ are the positions obtained through the transformation (3) as

$$\tilde{q}_i=\sqrt{\frac{2}{N}}\tilde{Q}_k\sin\left(\frac{\pi k}{N}i\right) \quad (i=1,2,\ldots,N-1), \tag{13}$$

and the components of $\tilde{\mathbf{p}}=(\tilde{p}_1,\ldots,\tilde{p}_{N-1})$ are the conjugate momenta. Since $\tilde{Q}_k(t)$ is an approximate rather than an exact solution, the periodic orbit $\tilde{\mathbf{\Gamma}}(t)$ is also only approximate. In this sense, we call $\tilde{\mathbf{\Gamma}}(t)$ a *pseudoperiodic orbit*. An orbit starting from a single-mode excitation condition may stay close to such a pseudoperiodic orbit during a certain short period, after which it will begin to diffuse in phase space. A schematic illustration of a pseudoperiodic orbit is shown in Fig. 1. The length of the period is characterized by τ_s; that is, τ_s is the time scale of the stability in phase space, over which the true orbits remain ''close'' to the pseudoperiodic orbit.

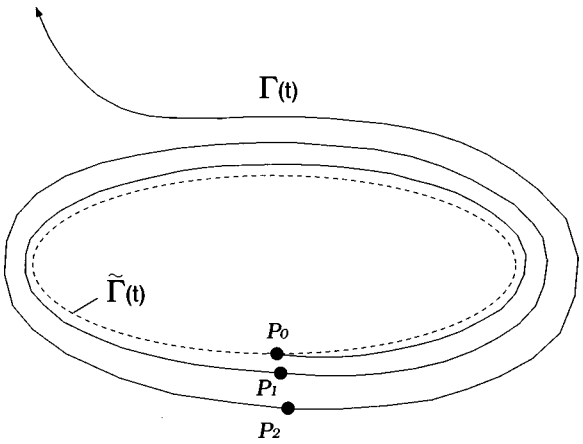

FIG. 1. Schematic illustration of a pseudoperiodic orbit. The actual orbit $\Gamma(t)$ remains close to the pseudoperiodic orbit $\tilde{\Gamma}(t)$ for a certain period $0<t<\tau_s$. After this time it diffuses in phase space.

B. Relaxation time

The time scale τ_s is estimated by the numerical integration of the equations of motion (2) to examine the stability of the normal mode. In this subsection, we describe how we estimate τ_s.

We define the harmonic energy E_i of each normal mode as

$$E_i(t)=\tfrac{1}{2}[\dot{Q}_i^2(t)+\omega_i^2Q_i^2(t)], \tag{14}$$

and the weights w_i, which give the fraction of the total harmonic energy in each normal mode by

$$w_i(t)=\frac{E_i(t)}{\sum_{m=1}^{N-1}E_m(t)}. \tag{15}$$

Let us define the spectral entropy $S(t)$ as [11]

$$S(t)=\sum_{i=1}^{N-1}-w_i(t)\ln w_i(t). \tag{16}$$

$S(t)$ can be normalized as

$$\eta(t)=\frac{S_{\max}-S(t)}{S_{\max}-S(0)}, \tag{17}$$

where $S_{\max}=\ln(N-1)$. The function $\eta(t)$ is used to measure the extent of the energy exchange among the normal modes. If there is no energy exchange among the normal modes, then $S(t)=S(0)$, and $\eta(t)$ remains unity. If energy ex-

change occurs, $\eta(t)$ decreases; $\eta(t)=0$ corresponds to the state in which energy is equally shared among all the normal modes. We define the relaxation time τ_R as the time at which $\eta(t)$ reaches a reference value of 0.6; i.e., $\eta(\tau_R)=0.6$. The time scale τ_s can be estimated by calculating the relaxation time τ_R defined above. We will use the inverse of the relaxation time, $1/\tau_R$, as an instability indicator. The choice of the reference value of $\eta(\tau_R)$ is somewhat arbitrary. We note, however, that the results of τ_R are not significantly affected by the choice of the reference value.

III. NUMERICAL EXPERIMENTS

We reported a strong wave-number dependence of the mode stability in our previous paper [20]. This finding was made only with respect to an FPU-β lattice with $N=128$. As mentioned in the Introduction, there is an open question concerning how the strong wave-number dependence of the mode stability is affected by an increase in the number of degrees of freedom.

We performed numerical experiments with different system sizes N in order to study the N dependence of the stability properties. The relaxation time τ_R has been calculated for various sets of k/N and ϵ. The calculation of τ_R was restricted to initial excitations of modes possessing odd wave numbers k, because if k is even the number of modes participating in the energy exchange with the initially excited mode, as determined by the selection rule (6), depends on k, while if k is odd, all the modes with odd wave number always participate.

Numerical integration of the equations of motion (2) was performed by the leap-frog algorithm because of its symplectic nature and simplicity. Allow us to briefly comment on the reliability of the numerical integration. To examine this reliability, we have used the fact that only normal modes of odd wave number are allowed to be excited when the initially excited mode has an odd wave number. The spectra of the harmonic energy E_i were examined at the ends of some runs. We confirmed that only the odd modes were excited, while the energy of the even modes was negligibly small. This fact supports the reliability of the numerical integration.

Figures 2–4 display the inverse of the relaxation time $1/\tau_R$ plotted against k/N and ϵ. Figures 2–4 represent the results for $N=128$, 256, and 512, respectively. The value $1/\tau_R$ is presented in Figs. 2(a), 3(a), and 4(a), and the contour plots are given in Figs. 2(b), 3(b), and 4(b). For a set of k/N and ϵ, we carried out the numerical integration for two sets of initial conditions with different phases of the single-mode excitation, one in which all the energy is contained in kinetic form, i.e., $Q_k(0)=0$, $\frac{1}{2}\dot{Q}_k^2(0)=E$, and one in which all the energy is contained in potential form, i.e., $\dot{Q}_k(0)=0$, $\frac{1}{2}\omega_k^2 Q_k^2(0)+(3\beta/8N)\omega_k^4 Q_k^4(0)=E$ [cf. Eq. (5)]. We found no significant difference between the relaxation times τ_R for these two sets of initial conditions. We defined the relaxation time τ_R for a given set of k/N and ϵ to be the average of the values found for these two sets of initial conditions. As noted above, the choice of the reference value of $\eta(\tau_R)$ is somewhat arbitrary. We changed the reference value in the range 0.4–0.7 and confirmed that the dependence of $1/\tau_R$ on both k/N and ϵ is not significantly affected by the choice of this reference value.

In the cases of $N=128$, 256, and 512, it is clearly seen that the stability of the normal mode is intricately dependent

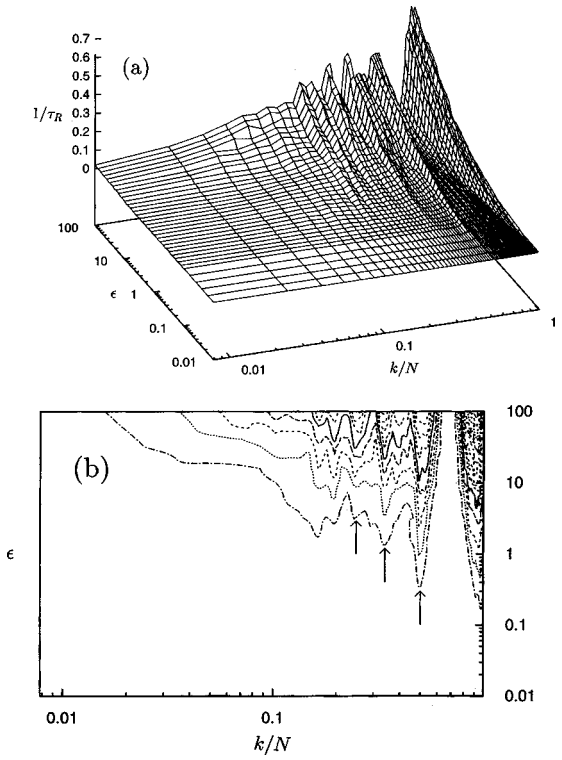

FIG. 2. (a) Inverse of the relaxation time, $1/\tau_R$, plotted as a function of ϵ and k/N. (b) Contour plot of the same quantity. The number of degrees of freedom here is $N=128$. Arrows indicate the peaks of $1/\tau_R$.

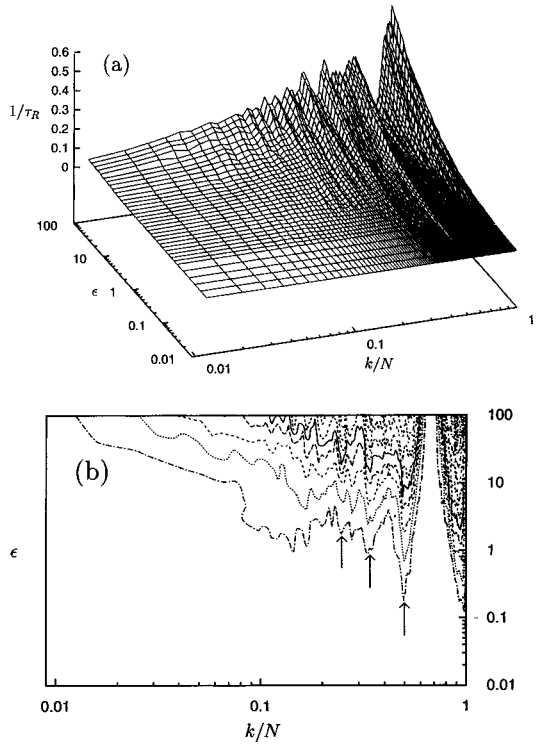

FIG. 3. Same as Fig. 2 for the case of $N=256$.

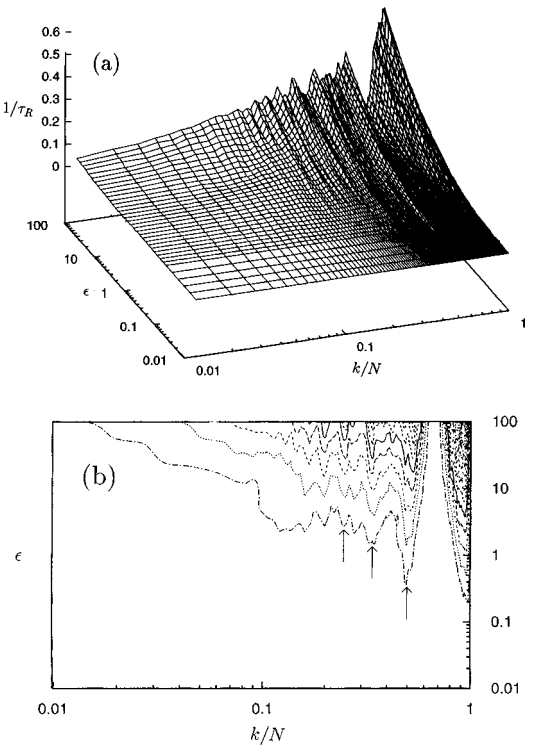

FIG. 4. Same as Fig. 2 for the case of $N=512$. To enhance the graphical presentation, averages of $1/\tau_R$ taken over two neighboring odd modes are plotted.

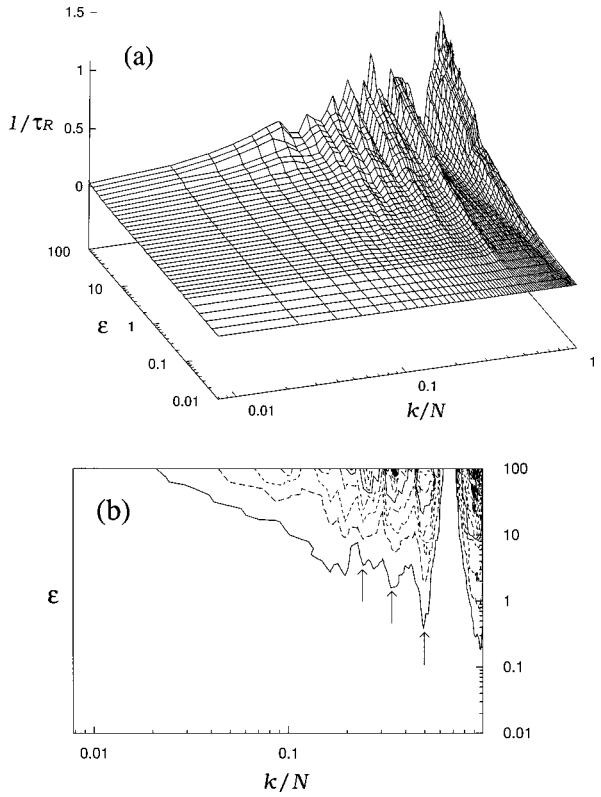

FIG. 5. Same as Fig. 2 for the case that a small amount of energy is initially placed on the two even modes next to the principally excited odd mode. A system size is $N=128$.

on the wave number. There is a particular interval of wave number values in which $1/\tau_R$ does not become large but remains remarkably small even at high energy density; i.e., the modes in this interval are not destabilized by an increase in the energy density. {We note that in low energy density regime, the values of τ_R for these modes are not relatively long compared with those of the other modes [this is consistent with Fig. 6(a)].} This interval of particular stability is located near $k/N \simeq 0.67$. We refer to this as a *stability band*. Some peaks of $1/\tau_R$ appear in ranges of wave numbers situated below the stability band. That is, the instability of the normal mode is enhanced intermittently in specific ranges of values of k/N corresponding to these peaks. We refer to the lines corresponding to these peaks as a *ridge structure*. The peaks of $1/\tau_R$ appear at $k/N \simeq 0.50$, 0.34, and 0.24. In the figures these peaks are indicated by the arrows, which are positioned at the same values of k/N. It should be noted that the values of k/N at which the stability band and the peaks of τ_R are located are identical for $N=128$, 256, and 512, showing no apparent dependence on N. These simulation results indicate that the stability of the normal mode depends on k/N, but not on k, and that the intricate dependence on k/N is relevant even in the thermodynamic limit $N \to \infty$.

The above numerical experiments dealt with the initial conditions for rigorous single-mode excitation. Normal modes of even wave number are never excited under those initial conditions. Therefore, the orbits are confined on the submanifold spanned by the odd modes' coordinates for all time. We carried out an additional numerical experiment in order to confirm that the observed strong wave-number dependence of mode stability is not caused by the confinement of orbits on the submanifold. In the additional numerical experiment, a small amount of energy is initially placed on the two even modes that are next to the principally excited odd mode: the energy of the principally excited odd mode and the neighboring even mode are set to $9.8 \times 10^{-1}E$ and $10^{-2}E$ at the initial, respectively. Normal modes of even wave number are also excited under this initial condition and therefore the orbit is not confined on the submanifold.

Figure 5(a) shows $1/\tau_R$ plotted against k/N and ϵ and the contour plot is shown in Fig. 5(b). The results are averaged over two sets of initial conditions with different phases of the principally excited odd mode as in the previous numerical experiments, one in which all the energy of the principally excited odd mode is contained in kinetic form, and one in which it is contained in potential form. For both of the sets of initial conditions, small amounts of energy of the neighboring even modes are contained in kinetic form.

The strong wave-number dependence of mode stability is clearly observed in the figure. Since η decreases faster under these sets of initial conditions than under the rigorous single-mode excitation, the values of $1/\tau_R$ are larger than those in Figs. 2–4. However, the wave-number dependence of mode stability coincides with those shown in Figs. 2–4 completely: peaks of $1/\tau_R$, which are indicated by arrows, and stability band appear at the same values of k/N. This result shows that the strong wave-number dependence of mode stability is not an artificial effect caused by the confinement of orbits on the submanifold.

IV. THEORETICAL ANALYSIS

A. Average variational equation

In this subsection, we introduce an *average variational equation* (AVE), which we propose as a theoretical tool for the stability analysis.

We defined the stability of the normal mode in terms of τ_s in the previous section. The stability time scale τ_s (or τ_R) is expected to be closely related to linear stability of an orbit with the relevant initial condition: exponential divergence of nearby orbits may be regarded as evidence for chaotic structure of the neighborhood of the orbit in phase space. In general, the presence of chaotic region in phase space is expected to yield faster diffusion of the orbit, implying faster energy exchange among the normal modes.

The close relation between the linear stability and the stability time scale may be justified by the following consideration (see Fig. 1). Let P_0 be an initial phase point of an orbit $\mathbf{\Gamma}(t)$ with single-mode excitation initial conditions (or almost single-mode excitation initial conditions including small perturbations, as in the case of Fig. 5) and $P_n, (n=1,2,\dots)$ be the phase points of $\mathbf{\Gamma}(t)$ at time $t=nT$, where T is the period of the pseudoperiodic orbit. Consider the orbit $\mathbf{\Gamma}(t;P_1)$ which has the initial point P_1 at $t=0$, i.e., $\mathbf{\Gamma}(t;P_1)=\mathbf{\Gamma}(t+T)$. Since P_1 is close to the initial point P_0, the time evolution of the difference between $\mathbf{\Gamma}(t)$ and $\mathbf{\Gamma}(t;P_1)$ is approximately described by the variational equation. Therefore, the ratio d_1/d_0 of distances, where d_i represents distance between P_i and P_{i+1}, is approximately given by the growth rate of a corresponding solution to the variational equation for the time interval T. Similarly, within the stability time scale $0<t<\tau_s$, where d_i is not so large, the other ratios $d_i/d_0, (i=2,3,\dots)$ are also approximately given by the growth rates for the time intervals iT. The distance between P_n and P_0 measuring separation of $\mathbf{\Gamma}(t)$ from P_0 for time interval nT is roughly estimated as $d_0+d_1+\cdots+d_{n-1}$. Therefore, larger growth rate of the solution to the variational equation implies faster separation of the orbit from its initial phase point. This consideration may support the close relation between the linear stability and the stability time scale.

As mentioned above, it is natural to consider the linear stability. Linear stability is examined by means of the variational equations which are obtained by linearizing the equations of motion (2). The variational equations are given in the vector form

$$\frac{d^2\boldsymbol{\xi}}{dt^2}+\underline{V}(\mathbf{q}(t))\boldsymbol{\xi}=\mathbf{0}, \tag{18}$$

where $\boldsymbol{\xi}$ represents variations in position, $\mathbf{q}(t)$ is the reference orbit generated by the equations of motion (2), and $\underline{V}(\mathbf{q}(t))$ is the $(N-1)\times(N-1)$ Hessian matrix for the potential function the elements of which are given by

$$[\underline{V}(\mathbf{q}(t))]_{ij}=\begin{cases} 2+3\beta[(q_i-q_{i+1})^2+(q_i-q_{i-1})^2], & i=j, \\ -1-3\beta(q_i-q_j)^2, & i=j\pm 1, \\ 0 \quad \text{otherwise}. \end{cases} \tag{19}$$

Linear stability can be quantified by the exponential growth rates of the solutions $\boldsymbol{\xi}(t)$ of Eq. (18).

Since we are interested in the stability time scale τ_s, exponential growth rates in the short period of time $t<\tau_s$ (rather than through infinite time) are useful. This fact enables us to simplify the variational equation (18). Any orbits starting with single-mode excitation initial conditions remain close to the pseudoperiodic orbit for $t<\tau_s$. In other words, the pseudoperiodic orbit approximates, in an average sense, the true orbit generated by the equations of motion (2) for the short period of time $t<\tau_s$. Therefore we replace the reference orbit $\mathbf{q}(t)$ in Eq. (18) by the pseudoperiodic orbit $\tilde{\mathbf{q}}(t)$ defined by Eq. (13). That is, the variational equation employed for the theoretical analysis is

$$\frac{d^2\boldsymbol{\xi}}{dt^2}+\underline{V}(\tilde{\mathbf{q}}(t))\boldsymbol{\xi}=\mathbf{0}. \tag{20}$$

We call this the ''average variational equation.'' All the elements of the matrix $\underline{V}(\tilde{\mathbf{q}}(t))$ are periodic since $\tilde{\mathbf{q}}(t)$ is a periodic function.

According to Floquet theory, Eq. (20) can have a solution that grows exponentially in time if the time evolution of $\underline{V}(\tilde{\mathbf{q}}(t))$ is of a suitable nature. The largest exponential growth rate λ_1 of the solution is useful to quantify the linear stability and estimated by

$$\lambda_1=\lim_{t\to\infty}\frac{1}{t}\ln\frac{\|\boldsymbol{\xi}(t)\|}{\|\boldsymbol{\xi}(0)\|}, \tag{21}$$

where $\|\boldsymbol{\xi}\|$ is the Euclidean norm of $\boldsymbol{\xi}$. The quantity λ_1 is called the *largest characteristic exponent* (LCE). We measure the linear stability by λ_1 for the purpose of understanding the intricate stability properties of the normal mode observed in the numerical experiments.

In principle, the original variational equation (18) should be used for linear stability analysis. However, it is not particularly useful to obtain a theoretical understanding of the essential mechanism which determines the stability properties of the normal mode, because detailed behavior of the true orbit $\mathbf{q}(t)$ generated by the equation of motion (2) is complicated and depends on each sampled reference orbit. It is necessary to make some approximation and simplification of the time dependence of the evolution matrix $\underline{V}(\mathbf{q}(t))$. Therefore, from a theoretical point of view, it is important to replace the true orbit $\mathbf{q}(t)$ by the pseudoperiodic orbit $\tilde{\mathbf{q}}(t)$. The AVE is more useful than the original variational equation for the purpose of obtaining a theoretical understanding because of the simplification resulting from this replacement; as will be shown, this replacement, accompanied by further approximation, makes it possible to show that the parametric instability mechanism plays a crucial role in determining the stability properties of the normal mode.

The AVE is, of course, not a variational equation in the usual sense. Thus one might claim that the AVE is inadequate and that the original variational equation must be used for linear stability analysis. However, we will show that the AVE is adequate to approximately describe linear stability

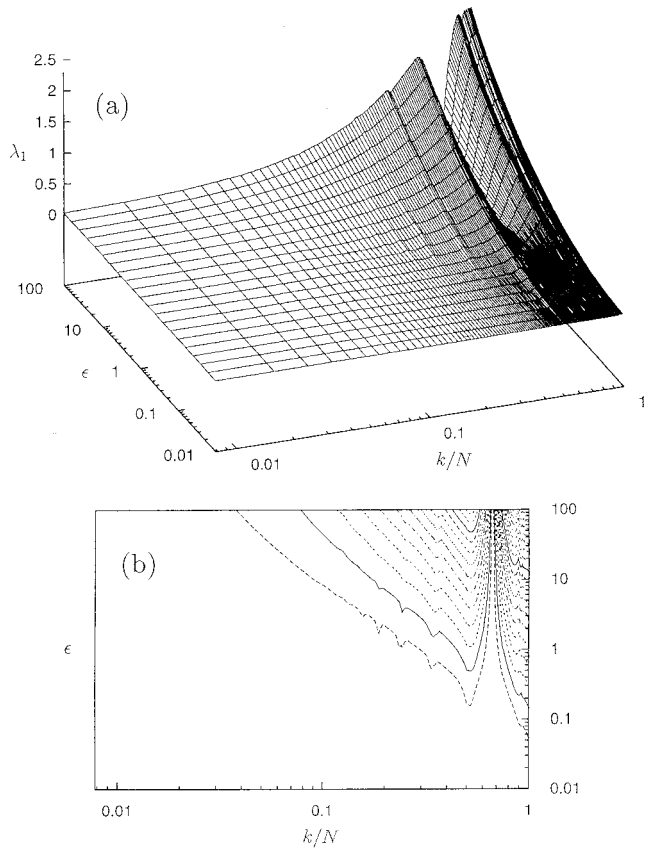

FIG. 6. (a) LCE λ_1 of AVE plotted as a function of ϵ and k/N. (b) Contour plot of the same quantity.

along the true orbits through a comparison between the results of the AVE and those of the original variational equation.

B. Results of AVE analysis

We have numerically calculated the LCE λ_1 of the AVE [Eq. (20)] for various sets of k/N and ϵ. The AVE used for the calculation corresponds to a lattice with $N=128$. The results are shown in Fig. 6, where the LCE is plotted as a function of k/N and ϵ, i.e., we consider $\lambda_1(k/N,\epsilon)$. The function $\lambda_1(k/N,\epsilon)$ is represented in Fig. 6(a), and the contour plot is given in Fig. 6(b). We also calculated the LCE for a few values of ϵ, with larger system sizes $N=256$ and 512 in order to examine the N dependence of the LCE. There was no apparent N dependence in the results: the LCE depends on k/N, but not on k. The k/N dependence of the LCE for $N=256$ and 512 was identical to that for $N=128$. This observation is consistent with the results for $1/\tau_R$ shown in the previous section.

The plot of λ_1 shown in Fig. 6(a) is quite similar to the plots of $1/\tau_R$ shown in Figs. 2(a), 3(a), 4(a), and 5(a). In the interval of the wave number corresponding to the stability band, located near $k/N\simeq 0.67$, λ_1 does not increase as the energy density increases, but rather remains remarkably small even in the high energy density regime. Some peaks of λ_1 are also found in wave-number ranges below the stability band. (This is the ridge structure mentioned above.) Three peaks of λ_1 are clearly seen near $k/N\simeq 0.50$, 0.34, and 0.24, and additional peaks, which are very weak, may be perceivable in smaller wave-number ranges. These three peaks appear at values of the k/N identical to those at which the peaks of $1/\tau_R$ are indicated in Figs. 2–5. The agreement between the AVE analysis and the numerical experiments establishes the close relation between the stability time scale τ_R and the linear stability along the pseudoperiodic orbit, and indicates that the features observed in the numerical experiments, namely the stability band and the ridge structure, can be well understood in terms of the LCE.

We now compare the LCE λ_1 with the largest exponential growth rate λ_1' of the solution of the original variational equation in order to confirm that the AVE is adequate for approximately describing the linear stability of the true orbits.

We first describe the method that numerically computes λ_1'. The original variational equation used for the comparison also corresponds to a lattice with $N=128$. The original variational equation has $2(N-1)$ independent solutions since it is a $(N-1)$-dimensional second-order differential equation. We can construct the $2(N-1)$ independent solutions $\boldsymbol{\xi}^{(n)}(t)[n=1,2,\ldots,2(N-1)]$ if we assume their initial conditions as

$$\xi_i^{(n)}(0)=\begin{cases}1, & i=n,\\ 0, & i\neq n,\end{cases}\qquad \dot{\xi}_i^{(n)}(0)=0\quad (n=1,\ldots,N-1), \tag{22}$$

and

$$\xi_i^{(n)}(0)=0,\quad \dot{\xi}_i^{(n)}(0)=\begin{cases}1, & i=n-(N-1)\\ 0, & i\neq n-(N-1)\end{cases}\quad [n=N,\ldots,2(N-1)], \tag{23}$$

where $\xi_i^{(n)}(i=1,\ldots,N-1)$ is the ith element of the vector $\boldsymbol{\xi}^{(n)}$. For a given reference orbit $\mathbf{q}(t)$ calculated from Eq. (2), the time evolution of these $2(N-1)$ solutions was numerically calculated according to Eq. (18), and the calculation was continued until the spectral entropy $\eta(t)$ reached 0.8. We denote the time at which the calculation was ended by τ_0; i.e., $\eta(\tau_0)=0.8$. It is reasonable to compare λ_1 with the value λ_1' calculated for the period in which large-scale energy exchange between the initially excited mode and the other modes does not take place, because the pseudoperiodic orbit is considered to approximate the true orbit only for the short period of time $0<t<\tau_s$. Therefore the reference value 0.8 of $\eta(\tau_0)$ was chosen to be close to 1. We define the matrix

$$\underline{R}=\begin{pmatrix} \xi_1^{(1)}(\tau_0) & \xi_1^{(2)}(\tau_0) & \cdots & \xi_1^{(2(N-1))}(\tau_0)\\ \vdots & \vdots & \ddots & \vdots\\ \xi_{N-1}^{(1)}(\tau_0) & \xi_{N-1}^{(2)}(\tau_0) & \cdots & \xi_{N-1}^{(2(N-1))}(\tau_0)\\ \dot{\xi}_1^{(1)}(\tau_0) & \dot{\xi}_1^{(2)}(\tau_0) & \cdots & \dot{\xi}_1^{(2(N-1))}(\tau_0)\\ \vdots & \vdots & \ddots & \vdots\\ \dot{\xi}_{N-1}^{(1)}(\tau_0) & \dot{\xi}_{N-1}^{(2)}(\tau_0) & \cdots & \dot{\xi}_{N-1}^{(2(N-1))}(\tau_0) \end{pmatrix}, \tag{24}$$

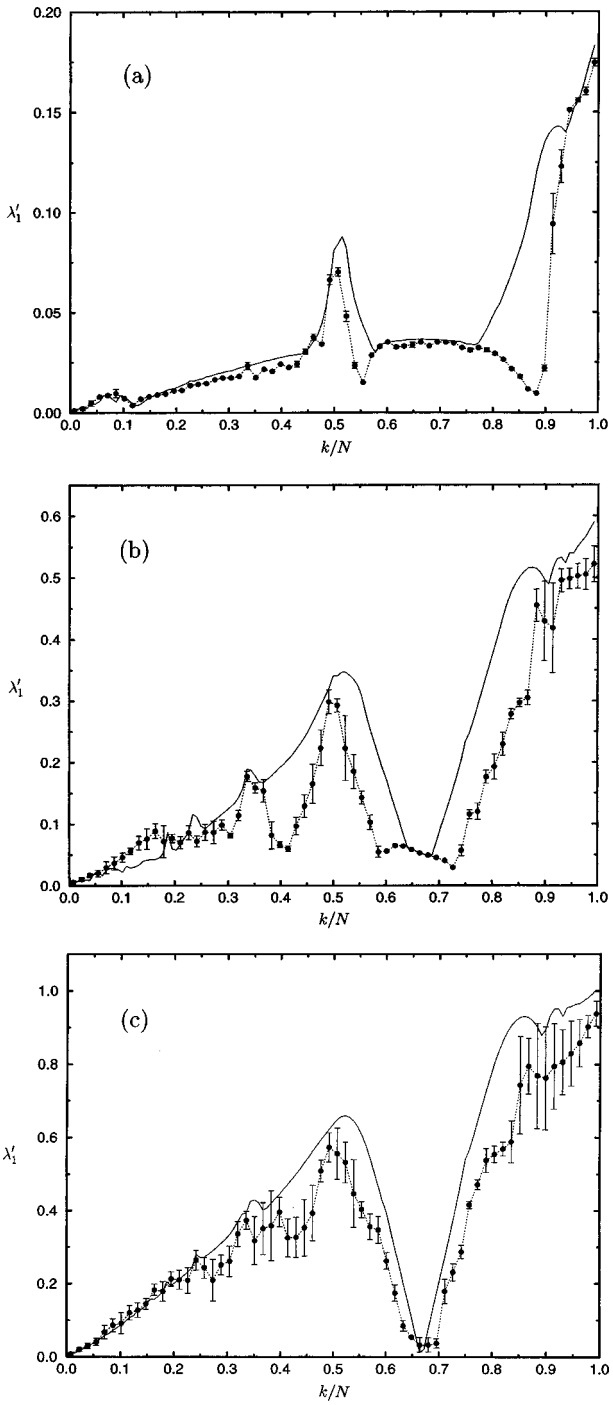

FIG. 7. The largest exponential growth rate λ_1' of the original variational equation vs k/N. LCE λ_1 (solid line) is compared with λ_1'. (a) $\epsilon=0.1$. (b) $\epsilon=1.0$. (c) $\epsilon=5.0$.

from the solutions $\boldsymbol{\xi}^{(n)}(\tau_0)$ at time τ_0. The value of λ_1' was determined from the largest eigenvalue ρ_R of the matrix R; i.e., $\lambda_1'=\ln|\rho_R|/\tau_0$. λ_1' determined by such a procedure depends on the reference orbit $\mathbf{q}(t)$ considered. We calculated λ_1' according to the above procedure for ten different reference orbits which were obtained by enforcing single-mode excitation initial conditions with different phases. We then averaged over the set of reference orbits.

Figures 7(a)–7(c) display λ_1' plotted against k/N for $\epsilon=0.1$, 1.0, and 5.0, respectively. λ_1' is represented by the solid circles with error bars, and the LCE λ_1 is also represented by the thin solid lines, where the error bars represent standard deviations.

The results show good agreement between λ_1 and the λ_1'. A small amount of discrepancy may be attributed to small-amplitude oscillations of modes other than the initially excited one. Even in the early stage of time evolution of the system, there occurs small-scale energy exchange between the initially excited mode and the other modes. The existence of the small-amplitude oscillations of the other modes, which is neglected in the pseudoperiodic orbit approximation, may be the reason for the difference in the value of λ_1 and λ_1'. In fact, the result for $\epsilon=0.1$ shows very good agreement between λ_1 and λ_1'. This is, no doubt, due to the fact that the energy exchange in this case of early time is smaller than in the other two cases.

The plots of λ_1' clearly exhibit the stability band structure: for values of k/N corresponding to the stability band, both λ_1' and λ_1 remains small when the energy density increases. The ridge structure can also be found in the plots of λ_1'. Figure 7(a) clearly shows the peaks of λ_1' at $k/N\simeq0.50$ and, though it is quite weak, also at $k/N\simeq0.34$. In Fig. 7(b), these two peaks appear more clearly, while the peak at $k/N\simeq0.24$, as expected from the AVE analysis and the numerical experiments, cannot be clearly discerned (it may be very weak). The peak at $k/N\simeq0.24$ can be seen in Fig. 7(c). We have also computed λ_1' with the different reference value $\eta(\tau_0)=0.6$, since the choice of $\eta(\tau_0)=0.8$ is somewhat arbitrary. Both the stability band and the ridge structure are clearly seen in the results for $\eta(\tau_0)=0.6$ also, though the agreement between λ_1 and λ_1', as expected, becomes worse.

The above comparison demonstrates that the AVE is adequate to approximately describe linear stability along the true orbits: i.e, the tangent properties of the pseudoperiodic orbits are similar to those of the true orbits. It must be emphasized that the contribution of the pseudoperiodic orbit to the time dependence of the evolution matrix $\underline{V}$ is dominant in determining the linear stability of the true orbits with single-mode excitation initial conditions.

Based on the AVE analysis, it can be concluded that the strong k/N dependence of the mode stability found in numerical experiments, namely the stability band and the ridge structure, is explained by the nature of the linear stability along the *pseudoperiodic* orbit. In particular, the stability band is characterized by a small exponential growth rate along this orbit.

C. Four-mode approximation of AVE

The validity of our use of the AVE was confirmed in the above. We now proceed to carry out further theoretical study on the basis of the AVE in order to understand a part of the mechanism causing the strong k/N dependence of the mode stability. In particular, we clarify the essential mechanism causing the instability enhancement at $k/N\simeq0.5$ and high stability in the stability band.

In the previous subsections, we used the AVE and the original variational equation which are expressed in the ordinary coordinates because of convenience for numerical calculation: a large number of interaction terms appear in the original variational equation if it is written in the normal

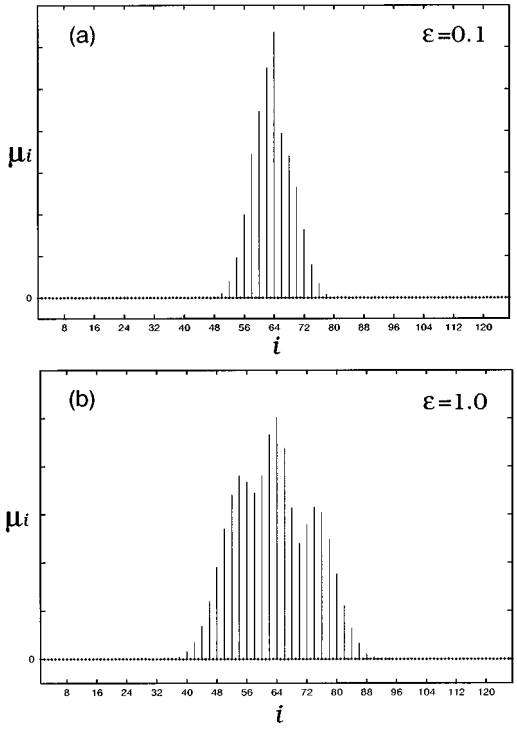

FIG. 8. Maximal values of mode components μ_i plotted against i for the case of $k=65$. The number of degrees of freedom here is $N=128$ (a) $\epsilon=0.1$. (b) $\epsilon=1.0$.

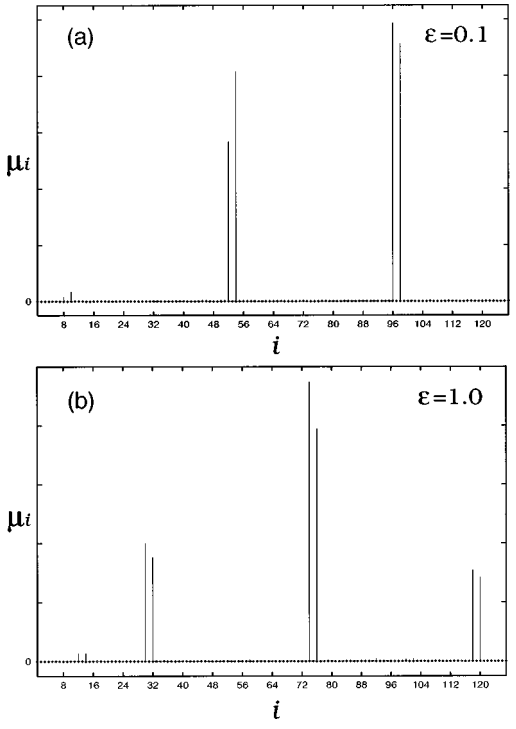

FIG. 9. Same as Fig. 8 for the case of $k=75$. (a) $\epsilon=0.1$. (b) $\epsilon=1.0$.

mode coordinates and it is cumbersome to calculate the true orbit in the normal mode coordinates by integrating Eq. (7). However, it is convenient to rewrite the AVE in the normal mode coordinates for understanding the mechanism responsible for the strong k/N dependence of the LCE. In this subsection, we rewrite the AVE and make a further simplification on it. We introduce the equations which are obtained by retaining only four important components in the AVE and truncating the others.

The AVE [Eq. (20)] is rewritten in the normal mode coordinates as

$$\frac{d^2}{dt^2}\hat{\xi}_i+\omega_i^2\hat{\xi}_i+\frac{3\beta}{2N}\omega_k^2\tilde{Q}_k^2\sum_{j=1}^{N-1}\omega_i\omega_j\hat{\xi}_j D(i,j,k,k)=0, \tag{25}$$

where k is the wave number of the initially excited mode and $\hat{\xi}_i$ represents a variation in the ith normal mode amplitude Q_i. The function $D(i,j,k,k)$ gives a coupling coefficient between mode components $\hat{\xi}_i$ and $\hat{\xi}_j$.

We numerically integrate Eq. (25) and calculate the variational vector $\hat{\boldsymbol{\xi}}$ which gives the LCE, in order to find out a set of a small number of mode components $\hat{\xi}_i$ which are important for describing the k/N dependence of the LCE, especially in the k/N range near the stability band ($0.5<k/N<0.9$). We started the numerical integration with initial conditions $\hat{\xi}_i(0)=0$ and $\dot{\hat{\xi}}_i(0)=1/\sqrt{N-1}$, and converged the vector $\hat{\boldsymbol{\xi}}(t)$ to that gives the LCE by iteratively normalizing its norm. In the numerical calculation, we set $N=128$. Figures 8, 9, and 10 show the maximal values that are taken by mode components of the vector $\boldsymbol{\mu}$, which is defined by $\boldsymbol{\mu}=\hat{\boldsymbol{\xi}}/\|\hat{\boldsymbol{\xi}}\|$, as a function of i for $k=65$, 75, and 85, respectively. It is found in the figures that most of μ_i are almost equal to zero and only a small number of components take nonnegligible values. This fact makes it possible to approximate the AVE by low-dimensional equations consisting of a few important mode components.

Figure 8 refers to the case of $k=65$ ($k/N\simeq0.51$). The normal mode of $k=65$ exhibits strong instability: a peak of the LCE appears near $k/N=0.5$ in Figs. 7(a) and 7(b), therefore the LCE for this mode is relatively large for both of the cases $\epsilon=0.1$ and 1.0. In Figs. 8(a) and 8(b), it is found that the mode components having nonnegligible values possess their indices i close to the initially excited mode's wave number $k=65$ for both $\epsilon=0.1$ and 1.0. It should be noted that four mode components with $i=60$, 62, 64, and 66 take large values in this case of large LCE. These four mode components are coupled in Eq. (25) as follows: two components of $i=64$ and 66, whose indices are next to the initially excited mode's wave number, are directly coupled to each other with nonzero coupling coefficient $D=1$ and the other two components of $i=62$ and 60 are directly coupled to $i=64$ and 66 with $D=-1$, respectively

Figure 10 refers to the case of $k=85$ ($k/N\simeq0.66$). The normal mode of $k=85$ is a highly stable one: the LCE for this mode remains small even for the larger energy density $\epsilon=1.0$ as seen in Fig. 7(b). In contrast to the case of $k=65$, spectra of $\boldsymbol{\mu}$ presented in Figs. 10(a) and 10(b) are quite different. The mode components with indices close to $k=85$ are almost equal to zero for both of the cases $\epsilon=0.1$ and 1.0. Two mode components with indices that are symmetrically far from $k=85$ take large values: the components of $i=69$ and 101 are large for $\epsilon=0.1$ and those of $i=67$ and 103 for $\epsilon=1.0$.

The normal mode of $k=75$ ($k/N\simeq0.59$) is of intermedi-

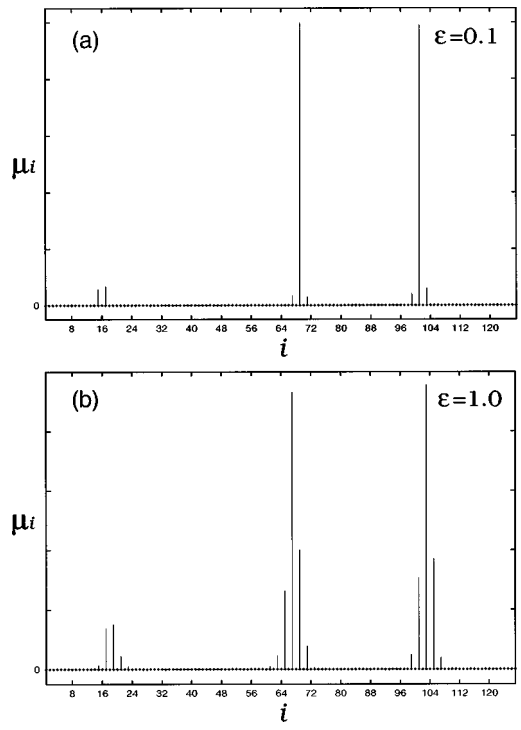

FIG. 10. Same as Fig. 8 for the case of $k=85$. (a) $\epsilon=0.1$. (b) $\epsilon=1.0$.

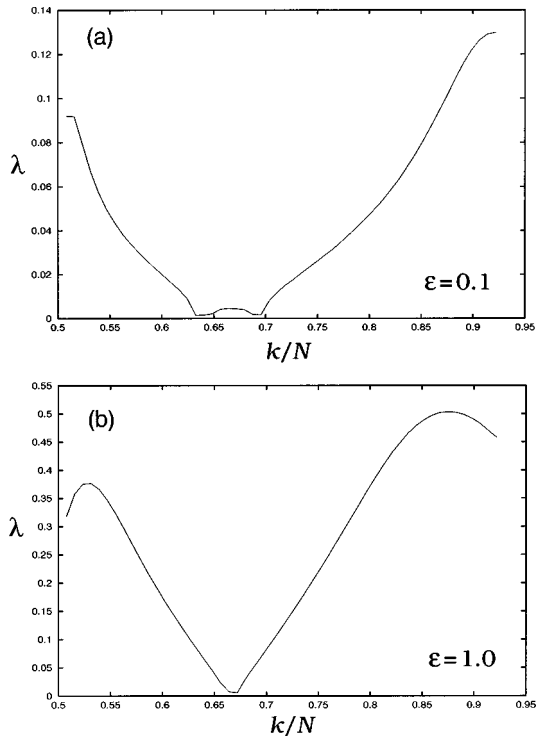

FIG. 11. The maximal exponential growth rate λ of Eq. (26) plotted against k/N. The number of degrees of freedom used in numerical calculation is $N=128$ (a) $\epsilon=0.1$. (b) $\epsilon=1.0$.

ate stability. This mode is not involved in the peak of LCE appearing around $k/N=0.5$ in Fig. 7(a) and thus the LCE for this mode is not relatively large when $\epsilon=0.1$. However, this mode comes to be involved in the peak in Fig. 7(b) and the LCE becomes relatively large when $\epsilon=1.0$. Correspondingly, the spectrum of $\boldsymbol{\mu}$ changes between the case of $\epsilon=0.1$ and 1.0, in Figs. 9(a) and 9(b). Spectrum for $\epsilon=0.1$ is similar to those observed in Figs. 10(a) and 10(b). The mode components of $i=54$ and 96, which are symmetrically far from the initially excited mode's wave number $k=75$, are large. In contrast to this, spectrum for $\epsilon=1.0$ is similar to those observed in Figs. 8(a) and 8(b). It is seen that four mode components of $i=30$, 32, 74, and 76 take large values for $\epsilon=1.0$. These four mode components are coupled in the same manner as in the case of $k=65$: two mode components of $i=74$ and 76, which are next to $k=75$, are directly coupled to each other with the coupling coefficient $D=1$ and the other two mode components of $i=32$ and 30 are directly coupled to $i=74$ and 76 with $D=-1$, respectively. It should be noted that these four mode components take large values when the LCE is relatively large.

Several peaks of LCE seen in Figs. 6(a) and 6(b) may be caused by some parametric instability mechanism because the AVE is a set of coupled Hill equations. The above observation shows that the LCE becomes large when the four mode components are dominant, while it cannot achieve a large value when the two mode components symmetrically far from k are dominant. Therefore, it is conceivable that a parametric instability due to interaction among those four mode components yields a large value of LCE, playing an important role in causing the peak of LCE appearing near $k/N=0.5$. We show that an analysis on the basis of equations consisting of the four dominant mode components can reveal the mechanism underlying the strong k/N dependence of LCE, i.e., the reasons why the LCE is maximized near $k/N=0.5$ and why the LCE is small near $k/N=0.67$.

The indices of the four dominant mode components are given by $i=k-1,k+1,|2N-3k+1|$, and $|2N-3k-1|$ as a function of the initially excited mode's wave number k. The mode components of $i=|2N-3k+1|$ and $|2N-3k-1|$ are directly coupled to the components of $i=k-1$ and $k+1$, respectively. If we retain only these four mode components in Eq. (25) then we have equations of the form

$$\frac{d^2}{dt^2}\hat{\xi}_{i_1}+\omega_{i_1}^2\hat{\xi}_{i_1}+\frac{3\beta}{2N}\omega_k^2\tilde{Q}_k^2 \times(2\omega_{i_1}^2\hat{\xi}_{i_1}+\omega_{i_1}\omega_{i_2}\hat{\xi}_{i_2}-\omega_{i_1}\omega_{i_3}\hat{\xi}_{i_3})=0,$$

$$\frac{d^2}{dt^2}\hat{\xi}_{i_2}+\omega_{i_2}^2\hat{\xi}_{i_2}+\frac{3\beta}{2N}\omega_k^2\tilde{Q}_k^2 \times(\omega_{i_1}\omega_{i_2}\hat{\xi}_{i_1}+2\omega_{i_2}^2\hat{\xi}_{i_2}-\omega_{i_2}\omega_{i_4}\hat{\xi}_{i_4})=0,$$

$$\frac{d^2}{dt^2}\hat{\xi}_{i_3}+\omega_{i_3}^2\hat{\xi}_{i_3}+\frac{3\beta}{2N}\omega_k^2\tilde{Q}_k^2(-\omega_{i_1}\omega_{i_3}\hat{\xi}_{i_1}+2\omega_{i_3}^2\hat{\xi}_{i_3})=0, \tag{26}$$

$$\frac{d^2}{dt^2}\hat{\xi}_{i_4}+\omega_{i_4}^2\hat{\xi}_{i_4}+\frac{3\beta}{2N}\omega_k^2\tilde{Q}_k^2(-\omega_{i_2}\omega_{i_4}\hat{\xi}_{i_2}+2\omega_{i_4}^2\hat{\xi}_{i_4})=0,$$

where i_1,i_2,i_3, and i_4 stand for $k-1,k+1,|2N-3k+1|$, and $|2N-3k-1|$, respectively.

We denote the maximal exponential growth rate of the solution to Eq. (26) by λ. Figures 11(a) and 11(b) display λ plotted against k/N for $\epsilon=0.1$ and 1.0, where λ is calculated for $N=128$. The results are in good agreement with those of the LCE shown in Figs. 7(a) and 7(b) although there is a difference in a range near $k/N=0.67$, where the two mode components with indices symmetrically far from k are more important than the four mode components included in Eq. (26). In Figs. 11(a) and 11(b), λ decreases as k/N increases up to $k/N\simeq 0.67$, above which it increases again. This agreement demonstrates the validity of Eq. (26) in describing the main feature of k/N dependence of the LCE in the range $0.5<k/N<0.9$, apart from the difference observed in the range where the two mode components are dominant. Here, we note that another type of parametric instability among the mode components may have to be considered in the other range of k/N.

We also calculated the spectrum of $\boldsymbol{\mu}$ and λ for larger system sizes $N=256$ and 512. It was observed that the same four mode components, $k-1,k+1,|2N-3k+1|$, and $|2N-3k-1|$, have large values when the LCE is large. The k/N dependence of λ is also in agreement with that of the LCE obtained from the full-dimensional AVE in the range $0.5<k/N<0.9$. This fact indicates that the four-mode approximation, Eq. (26), is valid for any N.

We now proceed to clarify the essential parametric instability mechanism in Eq. (26) that causes the strong k/N dependence of λ observed in Figs. 11(a) and 11(b). The frequencies $\omega_{i_1},\omega_{i_2},\omega_{i_3}$, and ω_{i_4} are given by $\omega_{i_1}=2\sin[\pi(k-1)/2N]$, $\omega_{i_2}=2\sin[\pi(k+1)/2N]$, $\omega_{i_3}=2\sin(\pi|2N-3k+1|/2N)$, and $\omega_{i_4}=2\sin(\pi|2N-3k-1|/2N)$. It should be noted that $\omega_{i_1}\simeq\omega_{i_2}\simeq\omega_k$ and $\omega_{i_3}\simeq\omega_{i_4}\simeq\omega$ for large N, where ω_k and ω are defined by $\omega_k=2\sin(\pi k/2N)$ and $\omega=2\sin(\pi|2N-3k|/2N)$. Therefore, we can approximate as $\omega_{i_1}=\omega_{i_2}=\omega_k$ and $\omega_{i_3}=\omega_{i_4}=\omega$. This approximation can be validated by a numerical calculation of Eq. (26) with the approximation $\omega_{i_1}=\omega_{i_2}=\omega_k$ and $\omega_{i_3}=\omega_{i_4}=\omega$. If we make the above approximation, introduce a new time variable $\tau=\omega_k t$, and rewrite the dependent variables by $\hat{\xi}_1^*$, $\hat{\xi}_2^*$, $\hat{\xi}_3^*$, and $\hat{\xi}_4^*$ in Eq. (26), then we obtain the equations

$$\begin{aligned}
&\frac{d^2}{d\tau^2}\hat{\xi}_1^*+\hat{\xi}_1^*+\frac{3}{2}\beta\phi^2(2\hat{\xi}_1^*+\hat{\xi}_2^*-r\hat{\xi}_3^*)=0,\\
&\frac{d^2}{d\tau^2}\hat{\xi}_2^*+\hat{\xi}_2^*+\frac{3}{2}\beta\phi^2(\hat{\xi}_1^*+2\hat{\xi}_2^*-r\hat{\xi}_4^*)=0,\\
&\frac{d^2}{d\tau^2}\hat{\xi}_3^*+r^2\hat{\xi}_3^*+\frac{3}{2}\beta\phi^2(-r\hat{\xi}_1^*+2r^2\hat{\xi}_3^*)=0,\\
&\frac{d^2}{d\tau^2}\hat{\xi}_4^*+r^2\hat{\xi}_4^*+\frac{3}{2}\beta\phi^2(-r\hat{\xi}_2^*+2r^2\hat{\xi}_4^*)=0,
\end{aligned}\tag{27}$$

where r is the ratio between ω and ω_k defined by

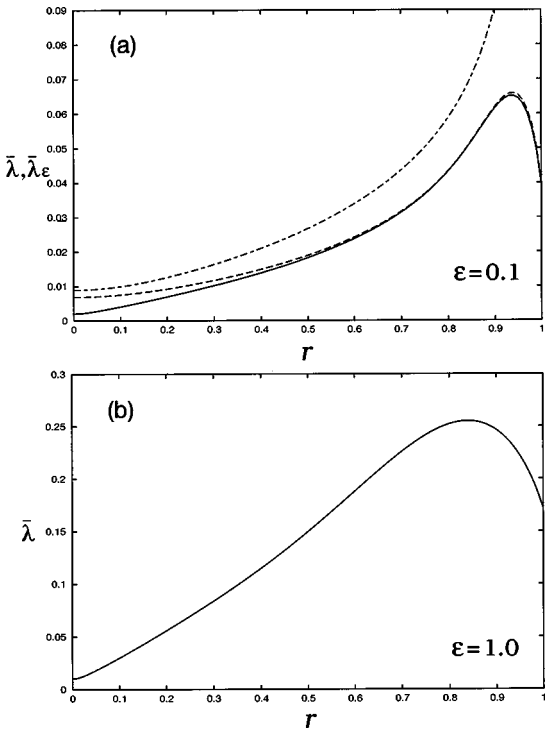

FIG. 12. The maximal exponential growth rate $\bar{\lambda}$ of Eq. (27) [or Eq. (31)] plotted as a function of the frequency ratio r by solid line. (a) $\epsilon=0.1$. (b) $\epsilon=1.0$. In (a), an analytical estimation $\bar{\lambda}_\epsilon$ for $\bar{\lambda}$ and a leading term in the expansion of $\bar{\lambda}_\epsilon$ are also plotted by the dashed line and dash-dotted line, respectively.

$$r=\frac{\omega}{\omega_k}=\frac{\sin\left(\frac{\pi}{2}\left|2-3\frac{k}{N}\right|\right)}{\sin\left(\frac{\pi k}{2N}\right)},\tag{28}$$

and the function $\phi(\tau)$ is defined as

$$\phi(\tau)=\frac{\omega_k}{\sqrt{N}}\tilde{Q}_k(\tau/\omega_k)=A\,\mathrm{cn}[(1+6\beta\epsilon)^{1/4}\tau,k_m],\tag{29}$$

where k_m is the modulus defined by Eq. (12) and the amplitude A is given by

$$A^2=\frac{2}{3\beta}(-1+\sqrt{1+6\beta\epsilon}).\tag{30}$$

The function ϕ does not depend on both k and N.

If we introduce new variables $\zeta_1=\hat{\xi}_1^*-\hat{\xi}_2^*$, $\zeta_2=\hat{\xi}_3^*-\hat{\xi}_4^*$, $\zeta_3=\hat{\xi}_1^*+\hat{\xi}_2^*$, and $\zeta_4=\hat{\xi}_3^*+\hat{\xi}_4^*$, then Eqs. (27) are divided into two decoupled pairs of equations of the form

$$\begin{aligned}
&\frac{d^2}{d\tau^2}\zeta_1+\zeta_1+\frac{3}{2}\beta\phi^2(\zeta_1-r\zeta_2)=0,\\
&\frac{d^2}{d\tau^2}\zeta_2+r^2\zeta_2+\frac{3}{2}\beta\phi^2(-r\zeta_1+2r^2\zeta_2)=0,
\end{aligned}\tag{31}$$

and

$$\frac{d^2}{d\tau^2}\zeta_3+\zeta_3+\frac{3}{2}\beta\phi^2(3\zeta_3-r\zeta_4)=0,$$
$$\frac{d^2}{d\tau^2}\zeta_4+r^2\zeta_4+\frac{3}{2}\beta\phi^2(-r\zeta_3+2r^2\zeta_4)=0. \tag{32}$$

We denote the maximal exponential growth rate of the solution to Eq. (27) by $\bar{\lambda}$, which is related to λ as $\lambda=\omega_k\bar{\lambda}$. Equations (31) give the maximal exponential growth rate $\bar{\lambda}$. We calculated $\bar{\lambda}$ for various values of r by numerically integrating Eqs. (31). Figures 12(a) and 12(b) show $\bar{\lambda}$ plotted against r for $\epsilon=0.1$ and 1.0, respectively. $\bar{\lambda}$ shows a maximum at $r\simeq 1$ and decreases as r decreases. $\bar{\lambda}$ has a very small value near $r=0$. A strong parametric instability occurs near $r=1$ while the parametric instability is suppressed near $r=0$.

If $r\simeq 0$, k/N satisfies the relation

$$\left|2-3\frac{k}{N}\right|\simeq 0. \tag{33}$$

from Eq. (28). Then, we obtain

$$\frac{k}{N}\simeq\frac{2}{3}. \tag{34}$$

And, if $r\simeq 1$, then k/N satisfies the relation

$$\left|2-3\frac{k}{N}\right|\simeq\frac{k}{N}. \tag{35}$$

One of the solutions to this equation is

$$\frac{k}{N}\simeq\frac{1}{2}. \tag{36}$$

The ratio r is equal to 1 at $k/N=1/2$ and decreases as k/N increases up to $k/N=2/3$, above which it increases again. Therefore, it may be concluded that the change of the intensity of parametric instability with varying r causes the strong k/N dependence of λ observed in Figs. 11(a) and 11(b), and hence that of the LCE λ_1. Since the correspondence between λ_1 and $1/\tau_R$ has already been demonstrated, the parametric instability which strongly depends on the ratio r provides the essential mechanism responsible for the strong k/N dependence of the stability time scale τ_R in the range $0.5<k/N<0.9$. As indicated by Eq. (34), the four-mode parametric instability is suppressed at $k/N\simeq 0.67$. Therefore, an instability caused by the interaction between the two mode components symmetrically far from k is dominant in the range near $k/N=0.67$. However, it cannot give rise to a strong instability even in a high energy density regime. This explains the appearance of the stability band at $k/N\simeq 0.67$. The enhancement of instability at $k/N\simeq 0.5$ is well explained by Eq. (36). This parametric instability mechanism of the four-mode approximation can explain also the fact that the mode stability depends on k/N, but not on k, because the ratio r is a function of k/N.

For small energy density ϵ, we can solve Eq. (31) analytically by means of the averaging method [21]. The analytical results provide more information. From Eq. (29), the period of the function ϕ is given by

$$T_\phi=\frac{4K(k_m)}{(1+6\beta\epsilon)^{1/4}}=\frac{4}{(1+6\beta\epsilon)^{1/4}}\int_0^{\pi/2}\frac{d\theta}{\sqrt{1-k_m^2\sin^2\theta}}, \tag{37}$$

where $K(k_m)$ represents the elliptic integral with modulus k_m defined by Eq. (12). The corresponding angular frequency is

$$\Omega=\frac{2\pi}{T_\phi}=\frac{\pi(1+6\beta\epsilon)^{1/4}}{2K(k_m)}. \tag{38}$$

Using the approximation $\phi(\tau)=A\cos(\Omega\tau)$, we bring Eq. (31) to the form

$$\frac{d^2}{d\tau^2}\zeta_1+\zeta_1\ +\gamma[1+\cos(2\Omega\tau)](\zeta_1-r\zeta_2)=0,$$
$$\frac{d^2}{d\tau^2}\zeta_2+r^2\zeta_2+\gamma[1+\cos(2\Omega\tau)](-r\zeta_1+2r^2\zeta_2)=0, \tag{39}$$

where the small parameter γ is defined by $\gamma=(3/4)\beta A^2$. We assume the solution to Eq. (39) in the form

$$\zeta_i=a_i(\tau)\sin(\Omega\tau)+b_i(\tau)\cos(\Omega\tau), \tag{40}$$

$$\frac{d\zeta_i}{d\tau}=\Omega a_i(\tau)\cos(\Omega\tau)-\Omega b_i(\tau)\sin(\Omega\tau), \tag{41}$$

where $i=1,2$. If we substitute Eqs. (40) and (41) into Eqs. (39) and average over the period $[0,T_\phi]$, we arrive at the averaged equations of the form

$$\frac{d}{d\tau}\begin{pmatrix}a_1\\b_1\\a_2\\b_2\end{pmatrix}=\frac{1}{4\Omega}\begin{pmatrix}0&2\Delta_{1a}&0&3\gamma r\\-2\Delta_{1b}&0&-\gamma r&0\\0&3\gamma r&0&2\Delta_{2a}\\-\gamma r&0&-2\Delta_{2b}&0\end{pmatrix}\begin{pmatrix}a_1\\b_1\\a_2\\b_2\end{pmatrix}, \tag{42}$$

where Δ_{1a}, Δ_{1b}, Δ_{2a}, and Δ_{2b} are defined as

$$\Delta_{1a}=\Omega^2-(1+\tfrac{3}{2}\gamma),\quad \Delta_{1b}=\Omega^2-(1+\tfrac{1}{2}\gamma),$$
$$\Delta_{2a}=\Omega^2-r^2(1+3\gamma),\quad \Delta_{2b}=\Omega^2-r^2(1+\gamma). \tag{43}$$

The largest eigenvalue $\bar{\lambda}_\epsilon$ of the coefficient matrix in Eq. (42) gives an approximate estimate of $\bar{\lambda}$ for small energy density ϵ. It can be explicitly obtained as

$$\bar{\lambda}_\epsilon=\frac{1}{4\Omega}[-3(\gamma r)^2-2(\Delta_{1a}\Delta_{1b}+\Delta_{2a}\Delta_{2b})+2\{(\Delta_{1a}+3\Delta_{2b})(\Delta_{2a}+3\Delta_{1b})(\gamma r)^2+(\Delta_{1a}\Delta_{1b}-\Delta_{2a}\Delta_{2b})^2\}^{1/2}]^{1/2}. \tag{44}$$

In Fig. 12(a), $\overline{\lambda}_\epsilon$ is plotted as a function of r by the dashed line. $\overline{\lambda}_\epsilon$ is in good agreement with $\overline{\lambda}$ although a slight difference is found near $r=0$, where the assumption Eqs. (40) and (41) does not give a good approximation. From Eq. (38), the frequency Ω can be expanded in powers of ϵ as

$$\Omega = 1 + \Omega_1 \beta\epsilon + \Omega_2 (\beta\epsilon)^2 + O(\epsilon^3) \tag{45}$$

$$= 1 + \tfrac{9}{8}\beta\epsilon - \tfrac{621}{256}(\beta\epsilon)^2 + O(\epsilon^3). \tag{46}$$

And, using Eq. (30), we can expand the parameter γ as

$$\gamma = \tfrac{3}{2}\beta\epsilon - \tfrac{9}{4}(\beta\epsilon)^2 + O(\epsilon^3). \tag{47}$$

Using Eqs. (45), (46), and (47), we obtain the expansion of Eq. (44), which is valid when r is not close to 1, to the leading order as

$$\overline{\lambda}_\epsilon = \frac{1}{8}\left\{ \frac{81}{4}(8\Omega_1 - 3)\frac{r^2}{1-r^2} - \frac{1}{2}(8\Omega_1^2 + 16\Omega_2 + 27)(8\Omega_1 - 3) \right\}^{1/2} (\beta\epsilon)^{3/2} + O(\epsilon^{5/2}), \tag{48}$$

$$= \frac{9}{8}\left\{ \frac{3r^2}{2(1-r^2)} + \frac{1}{16} \right\}^{1/2} (\beta\epsilon)^{3/2} + O(\epsilon^{5/2}). \tag{49}$$

In Fig. 12(a), the leading term in the expansion is plotted against r by the dash-dotted line for reference. This analytic expression clearly shows that $\overline{\lambda}_\epsilon$ increases rapidly as r becomes close to 1.

The LCE is approximately related to $\overline{\lambda}_\epsilon$ as $\lambda_1 \simeq \omega_k \overline{\lambda}_\epsilon$ in the regions where the four-mode parametric instability is dominant, i.e., in the peaks of the LCE situated on both sides of the stability band. Therefore, the above expression shows that the LCE increases in proportional to $\epsilon^{3/2}$ in those regions. It should be noted that the expansion coefficients of Ω are contained in the leading term in Eq. (48), particularly in the r-dependent term. This implies that the frequency shift of the initially excited mode due to the nonlinearity plays an important role in the k/N dependence of the LCE and subsequently in that of the mode stability, since the main feature of the k/N dependence of the LCE is well described by the four-mode approximation of the AVE. Therefore, one must take into account the frequency shift when studying the mode stability.

At the end of this section, we mention some remarks. We note that odd and even mode components are never coupled in Eq. (25) because of the nature of the function D. That is, the tangent subspace of odd components and that of even components are completely separated. As mentioned before, orbits are constrained on the submanifold spanned by the odd modes' coordinates for all time under rigorous single-mode excitation of an odd mode. Correspondingly, the stability time scale τ_R is related to the stability properties in the odd tangent subspace. In this case, parametric instability among the four odd mode components of $i=k-2$, $k+2$, $|2N-3k+2|$, and $|2N-3k-2|$ provides the essential mechanism responsible for the strong k/N dependence of τ_R because the four-mode components of $i=k-1$, $k+1$, $|2N-3k+1|$, and $|2N-3k-1|$ are even. The same parametric instability mechanism with the r-dependence can be applied to this case also.

Strong k/N dependence of the mode stability is reasonably expected to be generic to a large class of anharmonic lattice models (for instance, the ϕ^4 lattice, and the Lennard-Jones lattice in the case that the energy is small enough that the particles remain below the inflection point of the potential) because the AVE is always in the form of a set of coupled Hill equations and parametric instability is the common origin of instability. Since the parametric instability mechanism is associated with the detailed structure of the interaction rule among the normal modes, the k/N dependence of the mode stability may be model dependent.

V. CONCLUSIONS

The stability of normal modes was studied for the FPU-β lattice. This stability depends intricately on the wave number k/N. We have found that the mode instability is enhanced intermittently in some specific ranges of k/N. In addition, we have found that normal modes within the stability band remain extremely stable when the energy density increases.

The numerical experiments we carried out, possessing system sizes N in the range 128–512, indicate that there is no apparent N dependence in the intricate k/N-dependence of the mode stability. This fact coincides with the results obtained by the analysis using the four-mode approximation of the AVE. Therefore, it is indicated that the intricate stability properties persist even in the thermodynamic limit $N \to \infty$.

We investigated the mode stability by means of the linear stability analysis of the relevant orbits. Close relation between the stability time scale τ_R and the linear stability was established. We proposed the AVE as a theoretical tool for stability analysis and confirmed its reliability by comparing the largest exponential growth rates of the variations between the true orbits generated by the equations of motion and the pseudoperiodic orbits. The stability analysis based on the AVE shows that the strong k/N dependence of the mode stability found in the numerical experiments can be understood in terms of the linear stability along the pseudoperiodic orbits.

In order to facilitate theoretical study of the mechanism that causes the strong k/N dependence of the mode stability, we introduced the four-mode approximation of the AVE, which was obtained by truncating the other modes less important. The four-mode approximation consists of the two mode components the indices of which are next to the initially excited mode's wave number and the other two that are directly coupled to them through the interaction rule D. The frequencies of the former pair of mode components are approximately equal to $\omega_k = 2\sin(\pi k/2N)$ and those of the latter pair are approximately equal to $\omega = 2\sin(\pi|2N-3k|/2N)$. It was shown that the parametric instability that depends on the ratio of the above two frequencies, $r = \omega/\omega_k$, is the essential mechanism causing the strong k/N dependence of the mode stability in the range $0.5 < k/N < 0.9$: the enhancement of the mode instability near $k/N = 0.5$ is attributed to the strong parametric instability occurring when $r \simeq 1$, while the appear-

ance of the stability band near $k/N=0.67$ is attributed to the suppression of the parametric instability occurring when $r \simeq 0$. The analytical result obtained by the averaging method shows that the frequency shift in the initially excited mode oscillation plays an important role in the k/N dependence of the LCE and subsequently in that of the mode stability, implying that one must take into account the frequency shift when studying the mode stability.

Since the parametric instability mechanism is the common origin of the instability in many models, it is expected that the strong k/N dependence of the mode stability we have observed in the present study is generic and observable in the other anharmonic lattice models although the type of k/N dependence is model dependent.

[1] E. Fermi, J. Pasta, and S. Ulam, *Collected Papers of E. Fermi*, edited by E. Segré (University of Chicago, Chicago, 1965).
[2] N. J. Zabusky and M. D. Kruskal, Phys. Rev. Lett. **15**, 240 (1965).
[3] F. M. Izrailev and B. V. Chirikov, Dokl. Akad. Nauk SSSR **166**, 57 (1966) [Sov. Phys. Dokl. **11**, 30 (1966)].
[4] G. P. Berman and A. R. Kolovskij, Zh. Éksp. Teor. Fiz. **87**, 1938 (1984) [Sov. Phys. JETP **60**, 1116 (1984)].
[5] N. Budinsky and T. Bountis, Physica D **8**, 445 (1983).
[6] R. L. Bivins, N. Metropolis, and J. R. Pasta, J. Comput. Phys. **12**, 65 (1973).
[7] C. F. Driscoll and T. M. O'Neil, Phys. Rev. Lett. **37**, 69 (1976).
[8] N. Saito, N. Ooyama, Y. Aizawa, and H. Hirooka, Prog. Theor. Phys. Suppl. **45**, 209 (1970).
[9] N. Saito, N. Hirotomi, and A. Ichimura, J. Phys. Soc. Jpn. **39**, 1431 (1975).
[10] P. Bocchieri, A. Scotti, B. Bearzi, and A. Loinger, Phys. Rev. A **2**, 2013 (1970).
[11] M. Pettini and M. Landolfi, Phys. Rev. A **41**, 768 (1990).
[12] M. Pettini and M. Cerruti-Sola, Phys. Rev. A **44**, 975 (1991).
[13] H. Kantz, Physica D **39**, 322 (1989).
[14] H. Kantz, R. Livi, and S. Ruffo, J. Stat. Phys. **76**, 627 (1994).
[15] M. Pettini, Phys. Rev. E **47**, 828 (1993).
[16] L. Casetti and M. Pettini, Phys. Rev. E **48**, 4320 (1993).
[17] L. Casetti, R. Livi, and M. Pettini, Phys. Rev. Lett. **74**, 375 (1995).
[18] L. Casetti, C. Clementi, and M. Pettini, Phys. Rev. E **54**, 5969 (1996).
[19] G. M. Zaslawsky, *Chaos in Dynamic System* (Harwood Academic, Amsterdam, 1987).
[20] K. Yoshimura, Phys. Rev. E **54**, 5766 (1996).
[21] N. N. Bogoliubov and Y. A. Mitropolsky, *Asymptotic Methods in the Theory of Nonlinear Oscillations* (Gordon and Breach, New York, 1961).